Electric-field variations within a nematic-liquid-crystal layer

L. J. Cummings, E. Mema, C. Cai, and L. Kondic
Department of Mathematical Sciences and Center for Applied Mathematics and Statistics, New Jersey Institute of Technology, Newark, New Jersey 07102, USA
(Received 6 March 2014; published 3 July 2014)

A thin layer of nematic liquid crystal (NLC) across which an electric field is applied is a setup of great industrial importance in liquid crystal display devices. There is thus a large literature modeling this situation and related scenarios. A commonly used assumption is that an electric field generated by electrodes at the two bounding surfaces of the layer will produce a field that is uniform: that is, the presence of NLC does not affect the electric field. In this paper, we use calculus of variations to derive the equations coupling the electric potential to the orientation of the NLC's director field, and use a simple one-dimensional model to investigate the limitations of the uniform field assumption in the case of a steady applied field. The extension of the model to the unsteady case is also briefly discussed.

DOI: 10.1103/PhysRevE.90.012503 PACS number(s): 42.70.Df, 61.30.Dk, 61.30.Gd, 61.30.Hn

I. INTRODUCTION

With the current sustained demand for portable interactive electronic devices (phones, netbooks, music players, etc.) with liquid crystal displays (LCDs), there is considerable interest in understanding their operation from a theoretical perspective. Robust and accurate mathematical models for prototype LCDs allow simulations of hypothetical devices to be made quickly and at low cost, and this in turn can lead to new and potentially improved designs being identified. An example of this is the use of mathematical models to identify so-called *bistable* LCD designs [1–6]: such designs offer the potential for substantially lower power consumption as compared to traditional LCDs, with implications for battery lifetimes and portability, and possibly allowing LCD-based devices to compete with the "*e*-ink" technology [7] used in many *e*-readers.

Most models used in such theoretical investigations, including those referenced above, make several simplifications in order to arrive at a suitably tractable model for simulations. For example, normally an LCD device is, very reasonably, modeled as a layer of nematic liquid crystal (NLC) sandwiched between two parallel bounding plates, across which an electric field can be applied. Certain "anchoring" conditions on the molecules of the NLC are assumed at each bounding surface, which can be modeled by an appropriate surface energy (a macroscale modeling approximation to whatever microscopic interactions are really occurring at the interfaces). It is almost always assumed, since it facilitates the algebra immensely, that the Frank elastic constants appearing in the elastic energy [see Eq. (2) later] are equal (although they are not). Another key and widely used simplification is the assumption that, if the LCD is operated by an electric field applied across the parallel electrodes at the bounding surfaces, then the field generated within the NLC layer will be everywhere uniform and perpendicular to the electrodes, just as if the field was applied *in vacuo*. In reality, the molecules of the NLC contain electric dipoles that interact with the applied field, causing it to deviate from this uniform state. In this paper, we investigate the extent of such deviations under a range of operating conditions, and we address (partially) the issue of whether the deviations can become large, indicating breakdown of this commonly used assumption. This nonuniformity of the field in a NLC layer between parallel electrodes has certainly been studied before; see, for example, the book by Chigrinov [8] and many references therein. The particular contributions of this paper are as follows: first, to analyze theoretically the nonuniform field case in certain tractable asymptotic limits, to afford more insight into how and when deviations from the uniform field case arise; and second, to *quantify* the field nonuniformity in cases of industrial relevance, in order to assess the reasonableness of a uniform field approximation.

The paper is laid out as follows: In Sec. II, we introduce the key dependent variables, and outline the basic mathematical model in terms of free energy (Sec. II A), making clear any simplifying assumptions that are made. Section II B uses the calculus of variations to derive the coupled PDEs that govern the evolution of the director field of the NLC and the electric potential within the device. Section III describes briefly the approach taken to solve the coupled equations, and presents our key results. Finally, in Sec. IV we draw our conclusions.

II. MATHEMATICAL MODEL

Figure 1 shows the basic setup of the considered problem, consisting of a layer of nematic liquid crystal (NLC), sandwiched between parallel bounding surfaces at $z^* = 0$ and $z^* = h^*$, which also function as electrodes. Star superscripts will be used throughout to denote dimensional quantities, and will be dropped when we nondimensionalize. Throughout this study, we restrict attention to the steady situation in which no quantities vary in time, although we briefly discuss the extension to the time-dependent case.

The molecules of the NLC are rodlike, which imparts anisotropy. The polar molecules have a tendency to align locally, which is modeled by associating an elastic energy with any deviations from uniform alignment (see Sec. II A). The local average molecular orientation is described by a director field $\boldsymbol{n}$, a unit vector. We assume that properties of the bounding surfaces (electrodes) do not vary in the (x^*, y^*) plane, and we consider a purely one-dimensional (1D) model, within which (with appropriate choice of axes) the director is confined to a plane and may be expressed in terms of a single angle $\theta(z^*)$,

$$\boldsymbol{n} = (\sin\theta, 0, \cos\theta). \tag{1}$$

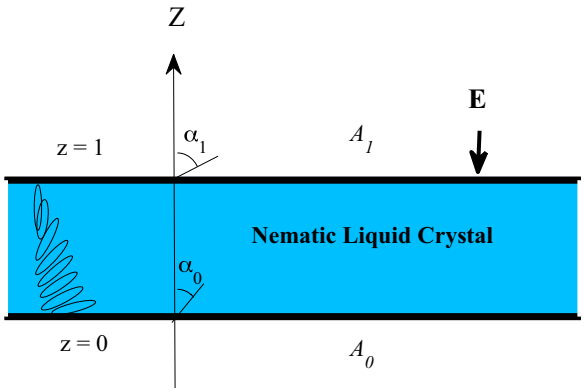

FIG. 1. (Color online) Sketch showing the setup and summarizing the key parameters in the dimensionless coordinates.

The director angle may vary across the layer in the z^* direction due to differences in the preferred substrate anchoring at the two boundaries, as discussed in the following.

We suppose that an electric field $\boldsymbol{E}^* = \nabla^*\phi^*$ is generated across the layer by applying a potential difference P^* across the plates, each being at fixed potential. Assuming that properties vary only in the z^* direction, $\phi^*(z^*)$ depends only on the coordinate z^*, and $\boldsymbol{E}^* = (0,0,\phi^*_{z^*})$. The function $\phi^*(z^*)$ is related to the usual electric potential V^* by $\phi^* = -V^*$; in the uniform field case $\phi^* \equiv P^* z^*/h^*$.

A. Energetics

The free energy of the liquid crystal layer, in the presence of an applied electric field and with specified anchoring conditions at each bounding surface, has several contributions. The bulk free energy density consists of elastic, dielectric, and flexoelectric contributions W_e^*, W_d^*, W_f^*, given (when the director is confined to a plane, allowing only bending and splaying) by

$$2W_e^* = K_1^*(\nabla^*\cdot\boldsymbol{n})^2 + K_3^*[(\nabla^*\times\boldsymbol{n})\times\boldsymbol{n}]^2, \tag{2}$$

$$2W_d^* = -\varepsilon_0^*(\varepsilon_\parallel - \varepsilon_\perp)(\boldsymbol{n}\cdot\boldsymbol{E}^*)^2 - \varepsilon_0^*\varepsilon_\perp \boldsymbol{E}^*\cdot\boldsymbol{E}^*, \tag{3}$$

$$W_f^* = -\boldsymbol{E}^*\cdot[e_1^*(\nabla^*\cdot\boldsymbol{n})\boldsymbol{n} + e_3^*(\nabla^*\times\boldsymbol{n})\times\boldsymbol{n}]. \tag{4}$$

Here, K_1^* and K_3^* are elastic constants, ε_0^* is the permittivity of free space, $\varepsilon_\parallel$ and $\varepsilon_\perp$ are the relative dielectric permittivities parallel and perpendicular to the long axis of the nematic molecules, and e_1^* and e_3^* are flexoelectric constants [9–11]. With the director field $\boldsymbol{n}$, as given by Eq. (1), and the very common simplifying assumption $K_1^* = K_3^* = K^*$, the total bulk free energy density $W^* = W_e^* + W_d^* + W_f^*$ simplifies. Introducing the nondimensional forms $W = W^* h^{*2}/K^*$, $\phi^* = P^*\phi$, and $z = z^*/h^*$,

$$W = \frac{1}{2}\theta_z^2 - \mathcal{D}\phi_z^2(\varpi + \cos^2\theta) + \frac{\mathcal{F}}{2}\theta_z\phi_z\sin 2\theta, \tag{5}$$

where

$$\mathcal{D} = \frac{P^{*2}\varepsilon_0^*(\varepsilon_\parallel - \varepsilon_\perp)}{2K^*}, \quad \mathcal{F} = \frac{P^*(e_1^* + e_3^*)}{K^*}, \quad \varpi = \frac{\varepsilon_\perp}{\varepsilon_\parallel - \varepsilon_\perp} \tag{6}$$

are dimensionless constants. With representative values $h^* \sim 2\ \mu$m, $P^* \sim 1$ V, $e_1^* + e_3^* \sim 5\times 10^{-11}$ C m^{-1}, $K^* \sim 1\times 10^{-11}$ N, $\varepsilon_\parallel - \varepsilon_\perp \sim 5$ [2,12,13], both $\mathcal{D}$ and $\mathcal{F}$ are $O(1)$. Note that these values are not intended to be absolute; a fair degree of variation is possible depending on the specific device design and indeed, many different combinations of dimensional parameter values will lead to the same model in dimensionless form. Note that $\mathcal{D}$ and $\mathcal{F}$ are not independent; the ratio

$$\Upsilon = \frac{\mathcal{F}^2}{\mathcal{D}} = \frac{2(e_1^* + e_3^*)^2}{K^*\varepsilon_0^*(\varepsilon_\parallel - \varepsilon_\perp)} \tag{7}$$

is a material parameter, independent of the applied field and of device geometry. We consider the most common case in which the dielectric anisotropy is positive: $\varepsilon_\parallel - \varepsilon_\perp > 0$ (molecules align parallel, rather than perpendicular, to an applied field), so that $\mathcal{D} > 0$ always. The parameter $\mathcal{F}$ characterizing the dimensionless strength of the applied electric field will, however, change sign if the electric-field direction is reversed. Since the representative parameter values listed above give $\Upsilon \approx 10$, we assign this value to Υ throughout most of our simulations.

The surface anchoring is modeled by the most commonly used Rapini-Papoular form [14]; if $g^*_{\{0,h^*\}} = (K^*/h^*)g_{\{0,1\}}$ are the surface energies per unit length at the boundaries $z^* = 0, h^*$, then

$$g_{\{0,1\}} = \frac{\mathcal{A}_{\{0,1\}}}{2}\sin^2(\theta - \alpha_{\{0,1\}}), \quad \mathcal{A}_{\{0,1\}} = \frac{h^* A^*_{\{0,h^*\}}}{K^*}, \tag{8}$$

where $A^*_{\{0,h^*\}}$ are the anchoring strengths at $z^* = 0, h^*$ and $\alpha_{\{0,1\}}$ are the preferred angles for the director at the respective boundaries. As $\mathcal{A}\to\infty$, the anchoring becomes strong, and the director angle is forced to take the value α. Figure 1 summarizes the setup and notation.

B. Calculus of variations

The total (dimensionless) free energy for the system, per unit area in the (x,y) plane, is given by

$$J[\theta,\phi] = \int_0^1 W(\theta,\theta_z,\phi_z)\,dz + g_0(\theta)|_{z=0} + g_1(\theta)|_{z=1} \tag{9}$$

and equilibrium solutions are those function pairs $\theta(z)$, $\phi(z)$ that minimize J, subject to the additional conditions $\phi = 0,1$ on $z = 0,1$. The standard calculus of variations approach, with $\theta(z)\mapsto\theta(z) + \epsilon\eta(z)$ and $\phi(z)\mapsto\phi(z) + \lambda\mu(z)$ $(0 < \epsilon,\lambda \ll 1)$ leads to $J \mapsto J[\theta + \epsilon\eta,\phi + \lambda\mu] = J_0 + J_1 + J_2 + O(\epsilon^3,\lambda^3)$, where $J_i = O(\epsilon^i,\lambda^i)$. For (θ,ϕ) to be a minimizing pair for J we require $J_1 = 0$, $J_2 > 0$, for all admissible variations η,μ (the condition on J_2 ensures we have a minimum, rather than a maximum, of the free energy). After Taylor expansion and integration by parts,

$$J_1 = \epsilon\int_0^1 \eta\big[W_\theta - \big(W_{\theta_z}\big)_z\big]dz - \lambda\int_0^1 \mu\big(W_{\phi_z}\big)_z\,dz + \epsilon\eta\big(g_{0\theta} - W_{\theta_z}\big)\big|_{z=0} + \eta\big(g_{1\theta} + W_{\theta_z}\big)\big|_{z=1}. \tag{10}$$

The condition that $O(\epsilon)$ and $O(\lambda)$ vanish independently for all admissible variations η,μ (admissible μ must vanish at $z = 0,1$ but admissible η need not) leads to the following

Euler-Lagrange equations for θ, ϕ [15]:

$$\theta_{zz} - \frac{\mathcal{F}^2}{\Upsilon}\phi_z^2 \sin 2\theta + \frac{\mathcal{F}}{2}\phi_{zz}\sin 2\theta = 0, \tag{11}$$

$$\frac{\mathcal{F}}{2}\theta_{zz}\sin 2\theta + \mathcal{F}\theta_z^2\cos 2\theta - \frac{2\mathcal{F}^2}{\Upsilon}\phi_{zz}(\varpi + \cos^2\theta) + \frac{2\mathcal{F}^2}{\Upsilon}\theta_z\phi_z\sin 2\theta = 0, \tag{12}$$

where we have eliminated $\mathcal{D}$ in favor of the material parameter Υ, reflecting the fact that $\mathcal{F}$ and $\mathcal{D}$ are not independent for a given device. These equations are solved subject to the following boundary conditions at $z = 0, 1$:

$$\theta_z + \frac{\mathcal{F}}{2}\phi_z\sin 2\theta - \frac{\mathcal{A}_0}{2}\sin 2(\theta - \alpha_0) = 0 \quad \text{on } z = 0, \tag{13}$$

$$\theta_z + \frac{\mathcal{F}}{2}\phi_z\sin 2\theta + \frac{\mathcal{A}_1}{2}\sin 2(\theta - \alpha_1) = 0 \quad \text{on } z = 1, \tag{14}$$

$$\phi = 0 \quad \text{on } z = 0, \tag{15}$$

$$\phi = 1 \quad \text{on } z = 1. \tag{16}$$

Conditions (13) and (14) arise from making the boundary terms vanish in Eq. (10). In the strong anchoring case $\mathcal{A}_0, \mathcal{A}_1 \to \infty$, these conditions naturally reduce to Dirichlet conditions on the director angle at each boundary. We note that Eq. (12) has the simpler integrated form

$$\frac{d}{dz}\left[\frac{\mathcal{F}}{2}\theta_z\sin 2\theta - \frac{2\mathcal{F}^2}{\Upsilon}\phi_z(\varpi + \cos^2\theta)\right] = 0. \tag{17}$$

However, the boundary conditions do not enable the constant of integration to be determined explicitly, and for practical purposes it is easier to solve the system of Eqs. (11)–(16) numerically using a standard boundary-value solver. Second, we emphasize that setting $\phi = z$ (the uniform field assumption) is *not* in general consistent with Eqs. (11)–(16). Nonetheless, the 1D uniform field model often used in practice is given by setting $\phi = z$ in Eqs. (11), (13), and (14) and neglecting Eqs. (12), (15), and (16).

Note that the second variation J_2 may be easily calculated for a range of suitable test functions if required to check stability. In practice, many of our steady states are found numerically using continuation methods from known "uniform field" steady states [3,15].

C. Time-dependent energetics: Gradient flow model

If the system is not initially at equilibrium, then it will evolve over time towards a steady state described by the above equations. An accurate description of these dynamics requires the full equations of nematodynamics [10,16], which couple flow to director reorientation, and the unsteady form of Maxwell's equations. The full time-dependent model would be extremely complicated, not to mention computationally intensive. Even with the uniform field assumption, many works [1–4,17] instead use a gradient flow model, which assumes that the system evolves always in the direction that minimizes its total free energy. In this simpler case [bulk and surface energy densities given by Eqs. (5) and (8), with $\phi \equiv z$], this process leads to [2–4,17]

$$\theta_t + \frac{\delta W}{\delta \theta} \equiv \theta_t + W_\theta - \left(W_{\theta_z}\right)_z = 0, \tag{18}$$

with dimensionless time $t = t^* K^*/(\tilde{\mu}^* h^{*2})$, where $\tilde{\mu}^*$ is the dimensional rotational viscosity of the NLC molecules (typically around 0.1 N s m^{-2}). Boundary conditions analogous to those specified by Eqs. (13) and (14) can also be written (see [2–4,17]), and an initial condition $\theta(z,0)$ closes the model.

With coupling to the electric field, matters are considerably more complicated. The above model (18) arises from a simple gradient flow for a one-component system. With two components (θ,ϕ) there is far more freedom, and any model of the form

$$\begin{pmatrix}\theta_t\\ \phi_t\end{pmatrix} + \underline{\underline{\mathbf{Q}}}\begin{pmatrix}\frac{\delta W}{\delta\theta}\\ \frac{\delta W}{\delta\phi}\end{pmatrix} = \underline{\mathbf{0}}$$

for positive definite $\underline{\underline{\mathbf{Q}}}$ (whose elements may depend on θ, ϕ) will evolve to the required steady states. (See [18] for a discussion of related issues for a two-component dissipative gradient dynamics formulation in a different fluid-dynamical context.) It is far from clear *a priori* what the physically appropriate choice of $\underline{\underline{\mathbf{Q}}}$ should be here. This question, while important, is beyond the scope of this paper, and henceforth we will restrict attention to the steady case described by Eqs. (11)–(16), which have a firm physical basis.

III. ANALYSIS AND RESULTS

The system of Eqs. (11)–(16) can be easily solved numerically and we present some steady solutions in Sec. III D. Before considering numerical results, however, we first discuss a number of analytical observations in Secs. III A–III C.

A. Large field limit

First, and as might be expected, the uniform field approximation is good in the large field limit $|\mathcal{F}| \gg 1$ [with $\Upsilon, \mathcal{A}_0, \mathcal{A}_1 \sim o(\mathcal{F})$]. In this case, treating $\mathcal{F}^{-1}$ as an asymptotically small parameter, and assuming regular series expansions for θ and ϕ in terms of $\mathcal{F}^{-1}$, Eqs. (11)–(16) become, to leading order,

$$\begin{aligned}
&\phi_{0z}^2 \sin 2\theta_0 = 0,\\
&\frac{d}{dz}[\phi_{0z}(\varpi + \cos^2\theta_0)] = 0,\\
&\phi_{0z}\sin 2\theta_0 = 0 \quad \text{on } z = 0,1,\\
&\phi_0 = 0,1 \quad \text{on } z = 0,1.
\end{aligned}$$

It is easily verified that all solutions of this system have the form

$$\phi_0 = z, \quad \theta_0 = 0 \ (\mathrm{mod}\pi/2). \tag{19}$$

In fact, the stable solutions (local minima, as opposed to local maxima, of the total free energy) are restricted to those with $\theta_0 = 0$ (modπ), but that does not affect our main conclusion, that correct to order $\mathcal{F}^{-1}$, the field is indeed uniform within the liquid crystal layer.

B. Small field limit

The story is rather different in the small field limit. Since this limit is of little practical use, we do not consider it in great detail, but present just two particular distinguished limits on the relative values of Υ and $\mathcal{F}$, that illustrate the field nonuniformity that can arise: Case 1, $\Upsilon \sim \mathcal{F} \ll 1$ and Case 2, $\Upsilon^{-1} \sim \mathcal{F} \ll 1$.

$$\text{Case 1: } \Upsilon \sim \mathcal{F} \ll 1$$

We write $\Upsilon = \mathcal{F}\tilde{\Upsilon}$, where $\tilde{\Upsilon} = O(1)$. Assuming regular asymptotic expansions for θ, ϕ in powers of $\mathcal{F} \ll 1$, Eqs. (11)–(16) become, to leading order,

$$\theta_{0zz} = 0, \tag{20}$$

$$\frac{d}{dz}\left[\frac{1}{2}\theta_{0z}\sin 2\theta_0 - \frac{2}{\tilde{\Upsilon}}\phi_{0z}(\varpi + \cos^2\theta_0)\right] = 0, \tag{21}$$

$$\theta_{0z} = \pm\frac{\mathcal{A}_{0,1}}{2}\sin 2(\theta_0 - \alpha_{0,1}) = 0 \quad \text{on} \quad z = 0,1, \tag{22}$$

$$\phi_0 = 0,1 \quad \text{on} \quad z = 0,1. \tag{23}$$

The problem for θ_0 decouples: θ_0 is linear in z, with coefficients determined by transcendental equations that follow from Eq. (22). With θ_0 known, we can solve for ϕ_0:

$$\phi_0 = \int_0^z \frac{k_1 + \tilde{\Upsilon}\theta_{0\xi}\sin 2\theta_0}{4(\varpi + \cos^2\theta_0)}d\xi, \quad k_1 = \frac{4 - \tilde{\Upsilon}\int_0^1 \frac{\theta_{0\xi}\sin 2\theta_0}{\varpi + \cos^2\theta_0}d\xi}{\int_0^1 \frac{d\xi}{\varpi + \cos^2\theta_0}}. \tag{24}$$

For the purposes of illustration, consider the specific case of strong anchoring, where $\mathcal{A}_{0,1} \to \infty$ [in fact, consistently with our asymptotic approximation we require only that $\mathcal{A}_{0,1}$ are $O(\mathcal{F}^{-1})$ or larger]; the details are qualitatively similar for the weak anchoring case. With strong anchoring,

$$\theta_0 = \alpha_0 + z(\alpha_1 - \alpha_0),$$

and the solution (24) is explicit. In this case, we see that, if $\alpha_0 = \alpha_1$, so that θ_0 is constant within the layer, we recover the uniform field $\phi_0 = z$. However, as the difference in anchoring angles increases, ϕ_0 departs from the linear state. Figure 2 shows the solution with $\alpha_0 = \pi/8$ and $\alpha_1 = 3\pi/8$: clearly, ϕ_0 is far from linear in this case.

We note that the chosen scaling of ϕ^* by the applied voltage P^*, while natural, has the effect of exaggerating the nonuniformities at small field since the dimensionless potential is always of order one. We return to this point in our numerical simulations of Sec. III D.

The director field is, however, largely unaffected by the nonlinearity in the electric potential, precisely because we considered the small field limit, which the director does not feel at leading order. Therefore, the conclusions in this case are unlikely to have any practical consequences.

$$\text{Case 2: } \Upsilon^{-1} \sim \mathcal{F} \ll 1$$

Given our estimate $\Upsilon \sim 10$ for a typical LCD device, a more relevant small field limit is to assume Υ to be asymptotically large: $\Upsilon = \mathcal{F}^{-1}\hat{\Upsilon}$, where $\hat{\Upsilon} = O(1)$. This should give some reasonable results for fixed, small values of $\mathcal{F}$. Examination of Eqs. (11)–(16) then reveals that the expansions for θ, ϕ must proceed as follows, with a rescaling of ϕ:

$$\theta = \theta_0 + \mathcal{F}\theta_1 + \ldots, \quad \phi = \mathcal{F}^{-1}\phi_0 + \phi_1 + \mathcal{F}\phi_2 + \ldots,$$

giving a leading-order system

$$\theta_{0zz} + \frac{1}{2}\phi_{0zz}\sin 2\theta_0 = 0, \quad \frac{d}{dz}[\theta_{0z}\sin 2\theta_0] = 0.$$

In the strong anchoring case $\mathcal{A}_{0,1} \gg \mathcal{F}^{-1}$, the boundary conditions on this leading order problem are

$$\theta_0 = \alpha_{0,1} \quad \text{on} \quad z = 0,1, \quad \phi_0 = 0 \quad \text{on} \quad z = 0,1.$$

The solution is straightforward:

$$\theta_0 = \tfrac{1}{2}\cos^{-1}[z(\cos 2\alpha_1 - \cos 2\alpha_0) + \cos 2\alpha_0], \tag{25}$$

$$\phi_0 = \frac{1}{4}\log\left[\frac{1 - (z-1)\cos 2\alpha_0 + z\cos 2\alpha_1}{1 + (z-1)\cos 2\alpha_0 - z\cos 2\alpha_1}\right] + \frac{1}{4}\log(\tan^2\alpha_0) + \frac{z}{4}\log\left[\frac{\tan^2\alpha_1}{\tan^2\alpha_0}\right]. \tag{26}$$

We can take the asymptotics further, noting that the problems for θ_1, ϕ_1 [given by $O(\mathcal{F})$ in Eq. (11) and $O(\mathcal{F}^2)$ in Eq. (12)] reduce to

$$\theta_{1zz} + \frac{1}{2}(\phi_{1zz}\sin 2\theta_0 + 2\theta_1\phi_{0zz}\cos 2\theta_0) = 0,$$

$$\frac{d^2}{dz^2}(\theta_1\sin 2\theta_0) = 0,$$

with boundary conditions

$$\theta_1 = 0 \quad \text{on} \quad z = 0,1, \quad \phi_1 = 0,1 \quad \text{on} \quad z = 0,1.$$

The solution is easily found as

$$\theta_1 = 0, \quad \phi_1 = z, \tag{27}$$

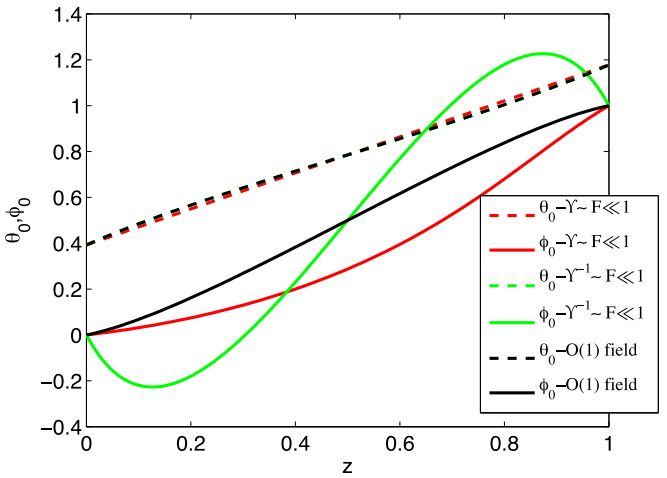

FIG. 2. (Color online) Leading order solutions for small field limit $\mathcal{F} \ll 1$, discussed in Sec. III B [Eq. (24), with $\tilde{\Upsilon} = 1$; and Eq. (28)]; and for $O(1)$ field case with $\Upsilon \gg 1$ (see Sec. III C) given by Eqs. (29) and (30), for $\mathcal{F} = 1$. All solutions use $\varpi = 0.25, \alpha_0 = \pi/8$, and $\alpha_1 = 3\pi/8$; anchoring is strong in all cases.

giving an improved approximation

$$\theta = \theta_0 + O(\mathcal{F}^2), \quad \phi = \frac{1}{\mathcal{F}}\phi_0 + \phi_1 + O(\mathcal{F}), \tag{28}$$

with θ_0, ϕ_0, and ϕ_1 given by Eqs. (25), (26), and (27).

Once again, for values of α_0 and α_1 that differ appreciably, ϕ_0 is highly nonlinear. Figure 2 shows the solution of Eq. (28) for anchoring angles $\alpha_1 = \pi/8$, $\alpha_2 = 3\pi/8$. Nonetheless, as in Case 1, even with this field nonuniformity, the asymptotic solution for θ is still quite close to the uniform field solution, both being close to linear. As the anchoring angles α_0, α_1 approach the same value, θ becomes constant and ϕ_0 approaches the uniform field solution $\phi_0 = z$.

In this strong anchoring limit, our asymptotic solution breaks down in the limit that α_0 and/or α_1 approach 0 or $\pi/2$. As this happens, boundary layers develop in the director solution: gradients of ϕ become very large near $z = 0,1$, and terms of size $\mathcal{F}\times$ (gradients of ϕ) that were initially neglected [in comparison with $O(1)$] in Eqs. (11) and (12) can no longer be ignored.

C. Order-one field, with $\Upsilon \gg 1$

As in Sec. III B, Case 2 above, we consider the parameter Υ to be asymptotically large, but now allow $\mathcal{F} = O(1)$ as will likely be the case during operation of a typical LCD device. In order to make analytical progress, we again consider the strong anchoring limit in which $\mathcal{A}_{0,1}$ are $O(\Upsilon)$ or larger. Assuming regular asymptotic expansions for θ and ϕ in inverse powers of Υ, the leading order equations and boundary conditions are almost the same as in Case 2 above:

$$\theta_{0zz} + \frac{\mathcal{F}}{2}\phi_{0zz}\sin 2\theta_0 = 0, \quad \frac{d}{dz}[\theta_{0z}\sin 2\theta_0] = 0,$$
$$\theta_0 = \alpha_{0,1} \quad \text{on} \quad z = 0,1, \quad \phi_0 = 0,1 \quad \text{on} \quad z = 0,1$$

(only a factor of $\mathcal{F}$, and the boundary condition on ϕ_0 at $z = 1$ differ). The solution is very similar:

$$\theta_0 = \frac{1}{2}\cos^{-1}[z(\cos 2\alpha_1 - \cos 2\alpha_0) + \cos 2\alpha_0], \tag{29}$$

$$\phi_0 = \frac{1}{4\mathcal{F}}\log\left[\frac{1-(z-1)\cos 2\alpha_0 + z\cos 2\alpha_1}{1+(z-1)\cos 2\alpha_0 - z\cos 2\alpha_1}\right] + \frac{1}{4}\log(\tan^2\alpha_0) + z\left(1 + \frac{1}{4\mathcal{F}}\log\left[\frac{\tan^2\alpha_1}{\tan^2\alpha_0}\right]\right). \tag{30}$$

The same comments apply as for the previous case: For values of α_0 and α_1 that differ appreciably, ϕ_0 is clearly nonlinear (see Fig. 2), while the leading order solution θ_0 is close to linear (as is the uniform field solution). As $\alpha_1 \to \alpha_0$, θ_0 becomes constant and ϕ_0 approaches the uniform field solution $\phi_0 = z$. This asymptotic solution breaks down in the limit that α_0 and/or α_1 approach 0 or $\pi/2$: gradients of ϕ become large in boundary layers near $z = 0,1$, and terms of size $\Upsilon^{-1}\times$ (gradients of ϕ) that were initially neglected in Eqs. (11) and (12) can no longer be ignored. Figure 2 shows the solution (29), (30) for anchoring angles $\alpha_1 = \pi/8$, $\alpha_2 = 3\pi/8$ (recall, anchoring is strong).

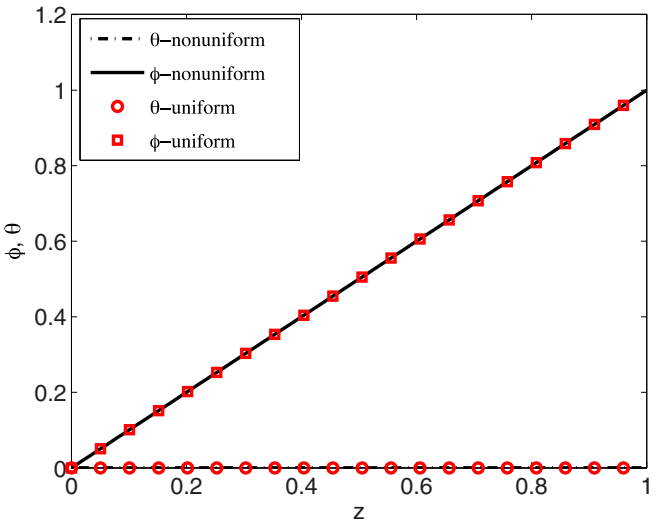

FIG. 3. (Color online) Comparison of the director field and electric potential with uniform and nonuniform field models at large field with weak anchoring: $\mathcal{F} = 10$, $\Upsilon = 2.5$, $\mathcal{A}_0 = 5.0$, $\mathcal{A}_1 = 2.4$, $\alpha_0 = 0$, $\alpha_1 = \pi/2$.

D. Numerical results

For other cases of interest where asymptotic progress is not possible, we solve the boundary-value problem specified by Eqs. (11)–(16) numerically. We first rewrite Eqs. (11) and (12) as a vector system of four first-order ordinary differential equations (ODEs) for θ, θ_z, ϕ, ϕ_z, and then apply the MATLAB routine bvp4c. An initial guess $[\theta_0(z),\phi_0(z)]$ is required to start the routine. For isolated calculations shown in Figs. 3–6, we take results from the analogous uniform field problem. For Figs. 7–10, which show the results of many calculations as the field strength $\mathcal{F}$ varies, we use uniform field results as the initial guess for the first point calculated, and continuation in $\mathcal{F}$ thereafter.

In this section, we use anchoring angles $\alpha_0 = 0$ and $\alpha_1 = \pi/2$, except if specified differently. This choice leads to particularly interesting results, first because the director varies maximally throughout the layer when the anchoring angles differ maximally, and second because there exist multiple director solutions that satisfy Eqs. (11)–(16). These include constant solutions $\theta = 0$, $\theta = \pi/2$ and a multiplicity of nontrivial solutions $\theta(z)$. However, only two solutions are reasonable candidates for free energy minimizers: the solution $\theta = 0$ and the particular nontrivial solution $\theta(z)$ that bends least between $z = 0$ and 1. Other nontrivial director solutions exist that rotate through angles larger than $\pi/2$ across the layer: such solutions are only stable because in our model the director is confined to the (x,z) plane; in a real three-dimensional (3D) setting, these states would "unwind" to a lower energy state. The $\theta = 0$ solution is curious because it is a "uniform field" solution of the full nonuniform field model: we refer to this solution as the "vertical solution" since the director field is purely vertical.

For surface anchoring strengths, we consider either strong anchoring, imposed in practice by setting $\mathcal{A}_0 = \mathcal{A}_1 = 1000$, or weak anchoring, with $\mathcal{A}_0 = 5.0$ and $\mathcal{A}_1 = 2.4$. The parameter ϖ is set to $\varpi = 0.25$ throughout.

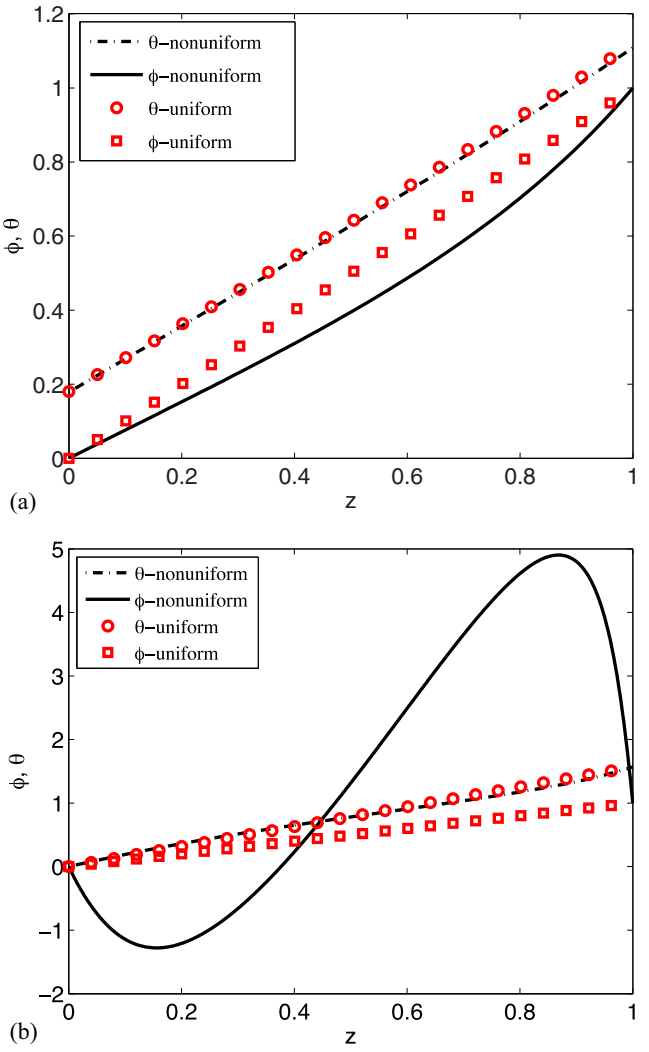

FIG. 4. (Color online) Comparison of the director field and electric potential with uniform and nonuniform field models at small field with (a) $\Upsilon \sim \mathcal{F} \ll 1$ and weak anchoring: $\mathcal{F} = -0.1$, $\Upsilon = 0.1$, $\mathcal{A}_0 = 5.0$, and $\mathcal{A}_1 = 2.4$; and (b) $\Upsilon \sim \mathcal{F}^{-1} \gg 1$ and strong anchoring: $\mathcal{F} = 0.1$, $\Upsilon = 10$, $\mathcal{A}_0 = \mathcal{A}_1 = 1000$. In both cases, $\alpha_0 = 0, \alpha_1 = \pi/2$.

We first consider solutions at large field. We know from the asymptotic result (19) that the uniform field approximation is good in this limit, so this serves as a useful crosscheck. We compare the solutions θ and ϕ for uniform and nonuniform electric fields. Specifically, in Fig. 3 we compare the uniform and nonuniform field cases with parameters $\mathcal{F} = 10$, $\Upsilon = 2.5$, $\mathcal{A}_0 = 5.0$, and $\mathcal{A}_1 = 2.4$. Clearly, agreement is excellent, as anticipated.

We next compare uniform and nonuniform field solutions in the small field limit. We know from the asymptotics of Sec. III B that we can expect significant deviation between uniform and nonuniform field solutions at small fields. Figure 4(a) shows the results with parameters $\mathcal{F} = -0.1$, $\Upsilon = 0.1$, $\mathcal{A}_0 = 5.0$, and $\mathcal{A}_1 = 2.4$. Note that although the nonuniform electric potential ϕ differs significantly from the linear case, the director field is largely unaffected by the nonlinearity of ϕ: as noted in Sec. III B earlier, this is precisely because we consider a small field, which the director does not feel at leading order. Figure 4(b) shows results with parameters $\mathcal{F} = 0.1$, $\Upsilon = 10$, $\mathcal{A}_0 = \mathcal{A}_1 = 1000$: the deviation of ϕ from the linear case is much more pronounced here.

Although the parameters used in Figs. 4(a) (weak anchoring, $\alpha_0 = 0, \alpha_1 = \pi/2$) and 4(b) (strong anchoring, $\alpha_0 = 0, \alpha_1 = \pi/2$) do not permit a direct comparison with the analytical results of Sec. III B, Cases 1 and 2 (Fig. 2: strong anchoring, $\alpha_0 = \pi/8$, $\alpha_1 = 3\pi/8$), the same qualitative features are observed in the numerics and the asymptotics. We note in particular that the boundary layers that were predicted in Sec. III B Case 2 for this choice of anchoring angles ($\alpha_0 = 0$, $\alpha_1 = \pi/2$) are evident in Fig. 4(b), particularly at $z = 1$. Numerical simulations (not shown) were also carried out for cases directly comparable to the asymptotics of Sec. III B, revealing good agreement with those results. As noted in that section, however, the scaling chosen for the electric potential assures that the dimensionless potential ϕ is always $O(1)$ even at small field, exaggerating the difference between the uniform and nonuniform field cases. When we calculate the deviations in the electric potential (Figs. 7 and 9 later) we therefore plot both the dimensionless and the dimensional deviations.

Since a typical LCD device operates in the regime $\mathcal{F} = O(1)$ and $\Upsilon \approx 10$, we take a closer look at the numerical results obtained with such parameter values. Given the asymptotic results of Sec. III C, for strong anchoring we expect the potential ϕ to be nonlinear, and the director solution θ to deviate from the uniform field solution. Figure 5 compares θ and ϕ for the uniform and nonuniform electric-field cases with strong anchoring at both boundaries. Parameter values here are chosen for direct comparison with the relevant asymptotic result shown in Fig. 2 (strong anchoring, with angles $\alpha_0 = \pi/8, \alpha_1 = 3\pi/8$). As anticipated, we now observe a measurable difference between the director solutions for uniform and nonuniform field cases, larger than in the previous two cases. Similar results are obtained when comparing the director solution and electric potential for weak anchoring

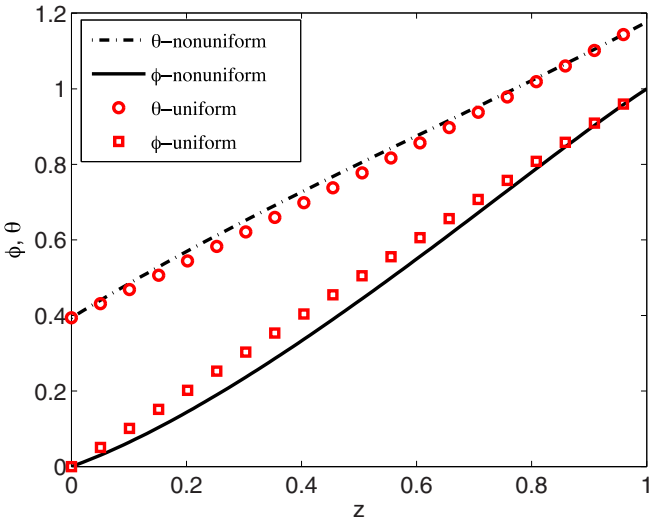

FIG. 5. (Color online) Comparison of the director field and electric potential with uniform and nonuniform field models at $O(1)$ field with strong anchoring: $\mathcal{F} = 1.0$, $\Upsilon = 10.0$, $\mathcal{A}_0 = \mathcal{A}_1 = 1000.0$, $\alpha_0 = \pi/8$, $\alpha_1 = 3\pi/8$.

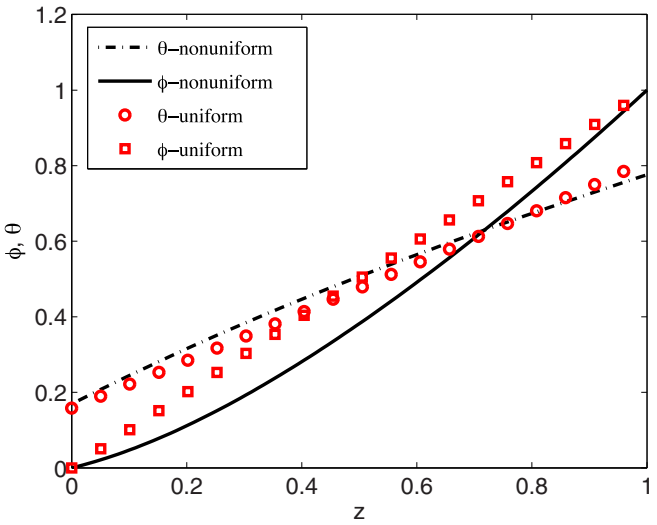

FIG. 6. (Color online) Comparison of the director field and electric potential with uniform and nonuniform field models at $O(1)$ field with weak anchoring: $\mathcal{F} = 1.0$, $\Upsilon = 10.0$, $\mathcal{A}_0 = 5.0$, $\mathcal{A}_1 = 2.4$, $\alpha_0 = 0$, $\alpha_1 = 3\pi/8$.

strengths. Figure 6 shows sample results for anchoring angles $\alpha_0 = 0$, $\alpha_1 = \pi/2$: again ϕ exhibits significant nonlinearity, and θ deviates measurably from the uniform field case.

Our results demonstrate that the uniform and nonuniform field cases may differ appreciably, which leads naturally to the following questions: (i) How large can the deviations between uniform and nonuniform field solutions be? (ii) Under what conditions can the uniform field assumption be considered reasonable? To begin to answer these questions, we measure the deviation between the potential ϕ (nonuniform electric-field model) and $\phi_{\text{unif}} = z$ (uniform electric-field model) as the electric-field strength parameter $\mathcal{F}$ varies. The deviation is calculated as a numerical approximation to the L_2 norm as follows:

$$\Delta\phi = \sqrt{\sum_{i=1}^{N}\left(\frac{(\phi_i - z_i)^2}{N}\right)},$$

where N is the number of points used in our numerical calculations; $\{z_i\}_{i=1}^{N}$ is the set of computational grid points, and ϕ_i is the approximation to the (nonuniform field) electric potential at the ith gridpoint. We also plot the analogous dimensional form of the deviation in the electric potential $\Delta\phi^*$ as well as the (dimensionless) deviations $\Delta\theta$ between the uniform and nonuniform field solutions for the director angle θ, calculated similarly. Since both ϕ and θ for the uniform field model (with the chosen anchoring conditions $\alpha_0 = 0$, $\alpha_1 = \pi/2$) have order-one averages ($\frac{1}{2}$ and $\pi/4$, respectively), we do not normalize the dimensionless deviations $\Delta\phi$, $\Delta\theta$ further.

Figures 7 and 8 illustrate the behavior of $\Delta\phi$ ($\Delta\phi^*$) and $\Delta\theta$ as $\mathcal{F}$ (P^*) varies for strong anchoring, with $\Upsilon = 10$. This strong anchoring case is relatively straightforward: we discuss first the deviations in the electric potential. As anticipated from the asymptotics of Sec. III B, deviations in the dimensionless potential ϕ are appreciable at small to moderate fields and, broadly speaking, decrease at larger field strengths [see

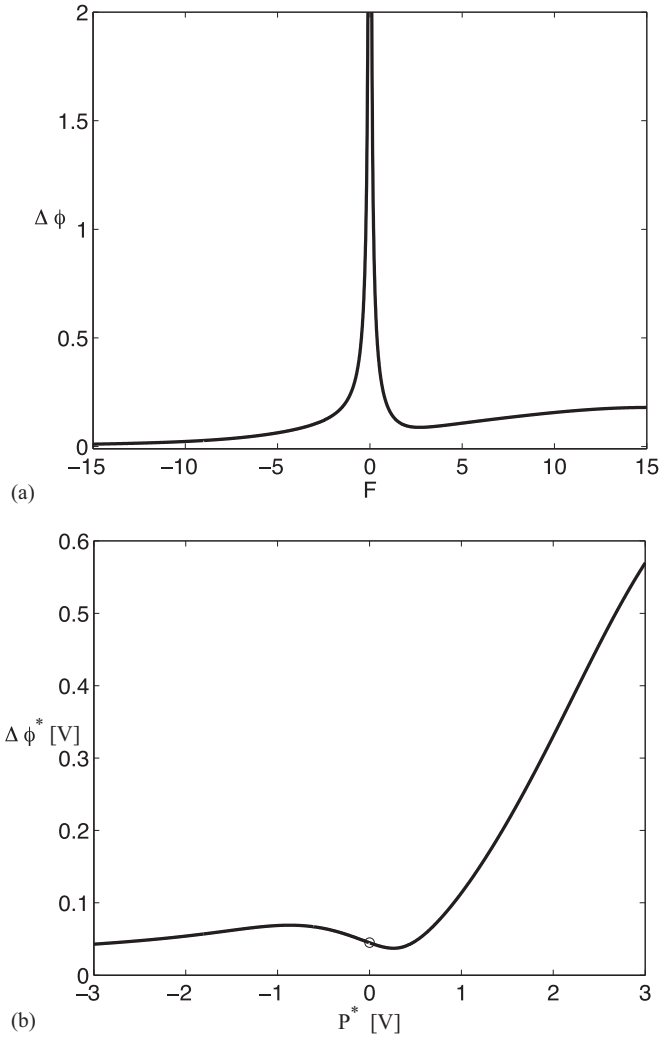

FIG. 7. (a) Deviation of the dimensionless electric potential ϕ from the uniform field case as $\mathcal{F}$ varies: $\Upsilon = 10.0$, $\mathcal{A}_0 = \mathcal{A}_1 = 1000.0$ (strong anchoring). (b) Deviation of the dimensional electric potential ϕ^* from uniform as the applied voltage P^* varies. The ranges of the two plots coincide. Further details are given in the text.

Fig. 7(a)]. For yet larger positive values of $\mathcal{F}$ (not shown), $\Delta\phi$ decreases slowly towards zero in line with the results of Sec. III A. The large deviations in ϕ at small fields may be understood in the light of the asymptotics of Sec. III B, Case 2, which demonstrates that $\Delta\phi$ is expected to be large for a large value of Υ when $\mathcal{F}$ is small. The plot of $\Delta\phi^*$ versus P^* [Fig. 7(b)] demonstrates that the blowup of $\Delta\phi$ at $\mathcal{F} = 0$ is an artifact of the scaling $\phi^* = P^*\phi$ that was employed in the nondimensionalization. This lower plot gives the absolute error in the uniform field approximation as a function of applied potential P^*, while the upper (dimensionless) plot may be interpreted as a measure of relative error (the error in the uniform field approximation relative to the applied potential).

Interestingly (although of course it does not make sense to plot the deviation in the solution for zero applied potential $P^* = 0$), we see that the absolute error in the uniform field approximation remains significant as $P^* \to 0$ (nonzero absolute error; large relative error). Figure 7(b) indicates that in fact $\Delta\phi^*$ approaches the same nonzero value as $P^* \to 0$

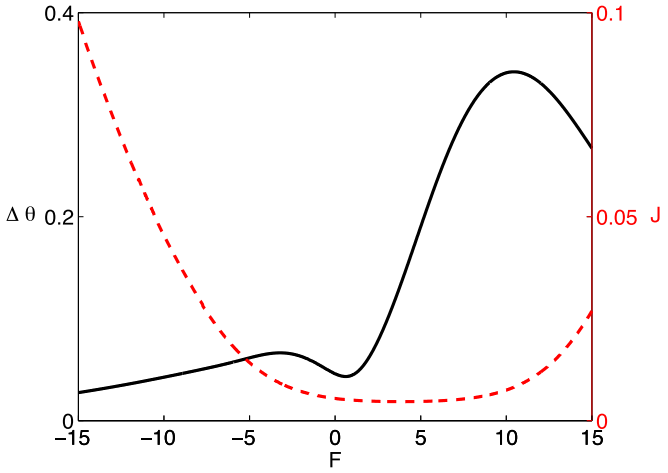

FIG. 8. (Color online) Deviation of the director angle θ (solid line) and total free energy J (dashed line) as $\mathcal{F}$ varies: $\Upsilon = 10.0$, $\mathcal{A}_0 = \mathcal{A}_1 = 1000.0$ (strong anchoring).

from either side (the circle at $P^* = 0$ indicates that the plot is undefined at that point). As $|P^*|$ increases, for negative values of P^* the absolute error $\Delta\phi^*$ decreases quickly and the relative error decreases faster still; for positive values of P^*, the absolute error $\Delta\phi^*$ is increasing, but ultimately the increase is sublinear, indicating the eventual decay of the relative error in the uniform field approximation.

Deviations in θ, as calculated for the uniform and nonuniform field models with strong anchoring, at first increase with $\mathcal{F}$ but then reach a maximum size, following which they decrease (see Fig. 8, solid curve). The deviations remain reasonably small for all $\mathcal{F}$ values considered. We note that the differences $\Delta\phi$, $\Delta\phi^*$, and $\Delta\theta$ never vanish in the strong anchoring case. Figure 8 also shows the dimensionless free energy of the nonuniform field solution [as defined by Eq. (9)], alongside the deviations in θ: the free energy exhibits fairly straightforward behavior, appearing rather flat for a range of $\mathcal{F}$ values, but then increasing monotonically as $|\mathcal{F}|$ becomes large. This is a consequence of the strong anchoring: the chosen director angles $\alpha_0 = 0$, $\alpha_1 = \pi/2$ are rigidly enforced at the boundaries $z = 0,1$, while the applied field acts to align the field along $\theta = 0$. This means that large distortions in θ are generated near $z = 1$ as $\mathcal{F}$ increases; these distortions are responsible for the increase in free energy.

Figures 9 and 10 present the results for the weak anchoring case. Focusing first on Fig. 9 we note that the behavior at small $\mathcal{F}$ is not significantly different in a qualitative sense to that observed in Fig. 7 for strong anchoring, with blowup in $\Delta\phi$ while the absolute deviation $\Delta\phi^*$ remains bounded. The size of the absolute deviation $\Delta\phi^*$ at small $\mathcal{F}$ is smaller with weak anchoring than with strong anchoring. This is because the electric field has a stronger effect (relative to the anchoring) near the boundaries in the weak anchoring case, so that the director will be more closely aligned with the field over the whole thickness of the layer, leading to smaller (although still nonzero) deviations from the uniform field. For $\mathcal{F} \gtrsim O(1)$ the behavior is more complex. While for negative values of $\mathcal{F}$ the deviations $\Delta\phi$, $\Delta\phi^*$ are always nonzero (at least for the values of $\mathcal{F}$, P^* considered), for positive $\mathcal{F}$ (P^*) there

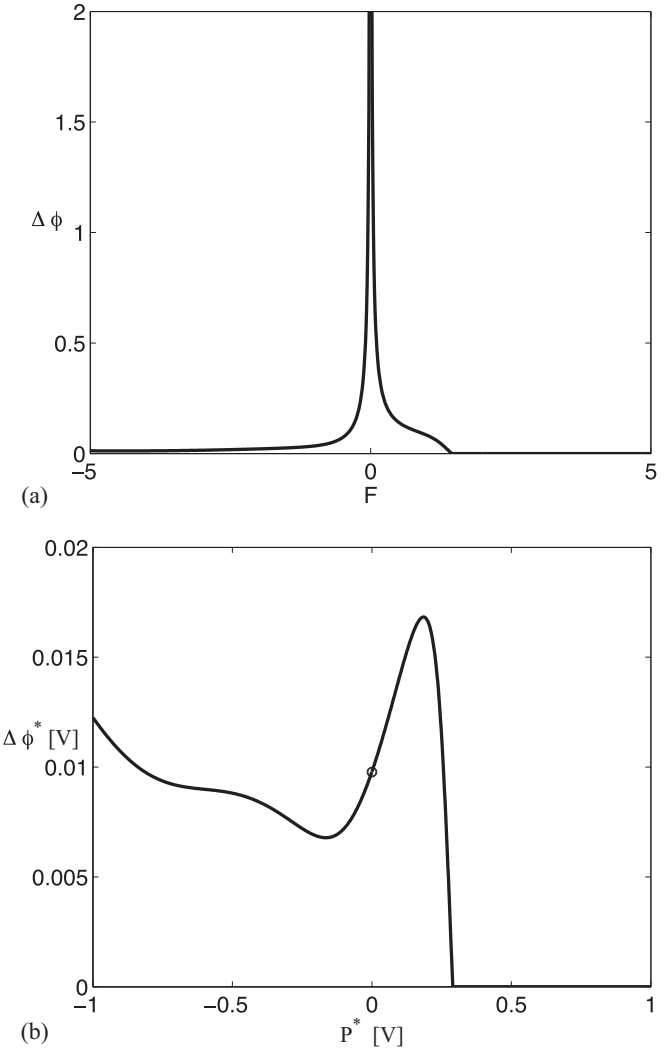

FIG. 9. (a) Deviation of the electric potential ϕ from the uniform field case as $\mathcal{F}$ varies: $\Upsilon = 10.0$, $\mathcal{A}_0 = 5.0$, and $\mathcal{A}_1 = 2.4$ (weak anchoring). (b) Deviation of the dimensional electric potential ϕ^* from uniform as the applied voltage P^* varies. The ranges of the two plots coincide. Further details are given in the text.

is a well-defined threshold value $\mathcal{F}_c \approx 1.45$ ($P_c^* \approx 0.29$ V) at which $\Delta\phi$ ($\Delta\phi^*$) drops abruptly to zero (see Fig. 9). This is strongly suggestive of a bifurcation in the solution. Returning to the full dimensionless model [Eqs. (11)–(16)], we observe that for this particular choice of anchoring angles $\alpha_0 = 0$, $\alpha_1 = \pi/2$, there is an exact "vertical" solution to the nonuniform field model: $\phi = z$ ($\phi^* = P^* z^*/h^*$), $\theta = 0$, in which both director and electric field are oriented exactly along the z axis. This is actually a "uniform field" solution to the "nonuniform field" model: To emphasize that we view it as a solution to the full nonuniform field model, we shall refer to it as the "vertical solution." At small positive $\mathcal{F}$, and for all negative $\mathcal{F}$ considered, this vertical solution is not the free energy minimizer, but for $\mathcal{F} > \mathcal{F}_c$ ($P^* > P_c^*$) it becomes so. We demonstrate this by plotting in Fig. 10 the deviations in director angle $\Delta\theta$ alongside the free energy [Eq. (9)] of the solution to the nonuniform field model. The free energy of the nonuniform field solution is initially smaller than that

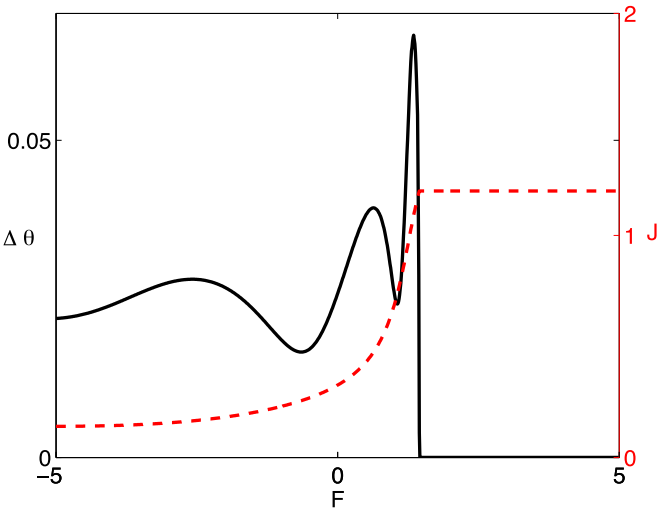

FIG. 10. (Color online) Deviation of the director θ (solid line) and total free energy J (dashed line) as $\mathcal{F}$ varies: $\Upsilon = 10.0$, $\mathcal{A}_0 = 5.0$, and $\mathcal{A}_1 = 2.4$ (weak anchoring).

of the vertical solution, but it increases monotonically with $\mathcal{F} > 0$. For $\mathcal{F} < \mathcal{F}_c$, the nonuniform field is the lowest energy solution, but at $\mathcal{F} = \mathcal{F}_c$ the nonuniform field solution's free energy becomes equal to the free energy of the vertical solution $\phi = z$, $\theta = 0$, and for $\mathcal{F} > \mathcal{F}_c$ exceeds it. At this value of $\mathcal{F}$, therefore, there is a bifurcation to the vertical solution (which, we emphasize, is an exact solution to the full nonuniform field model). The vertical solution, which has constant free energy independent of $\mathcal{F}$, then persists for all $\mathcal{F} > \mathcal{F}_c$.

Interestingly, the simpler uniform field model also permits two solutions in this weak anchoring case (one purely vertical, one not), and the bifurcation from the nonvertical to the vertical state appears to occur at almost exactly the same value $\mathcal{F}_c$. This observation (which we tested independently) is borne out by the transition in free energy of the two solutions taking place simultaneously with $\Delta\phi$ and $\Delta\theta$ dropping to zero (see Figs. 9 and 10). Both $\Delta\phi$ and $\Delta\theta$ being zero means that the solutions to uniform and nonuniform field models are identical, both being in the vertical configuration. For $\mathcal{F} < \mathcal{F}_c$, neither model is in the vertical state: both are in distinct nonvertical configurations. We conclude that both uniform and nonuniform field models exhibit the transition to the vertical state at the same value $\mathcal{F} = \mathcal{F}_c$. The significance of this finding will be considered in our future work.

IV. DISCUSSION AND CONCLUSIONS

We have used a steady state free energy minimization to derive a coupled system of equations for the director field and the electric potential within a confined layer of nematic liquid crystal. Our model describes the simplest possible case in which the layer is bounded by infinite parallel plates (the electrodes), and its properties vary only in the z direction, perpendicular to the plates. Our results reveal that, while the commonly used uniform field approximation (linear electric potential $\phi = z$) is fairly good in many situations of interest, there are parameter regimes in which ϕ can be visibly nonlinear. These deviations from the linear approximation were quantified in Figs. 7 and 9 for specific choices of parameter sets. A case for particular caution, given its likely physical relevance, is when the material parameter Υ defined in Eq. (7) is large, while the applied field [as characterized by the dimensionless parameter $\mathcal{F}$, see again Eq. (7)], is $O(1)$. In this case, we find that deviations of the electric field from the uniform case can be significant, as evidenced by Figs. 2, 4, 5, and 6. Figure 8 reveals that deviations in the director field θ (as predicted by the two models) can also be reasonably large in some regimes of interest, for example, when $\mathcal{F} \approx 10$. However, for order-one values of $\mathcal{F}$, Figs. 7 and 8 show that large deviations in ϕ can exist alongside acceptably small deviations $\Delta\theta$. Since the director orientation is often the key information desired in applications, this observation suggests that the uniform field approximation may in fact yield acceptable results even in situations when the field may be quite far from uniform.

ACKNOWLEDGMENT

This work was supported by the NSF under Grants No. DMS-0908158 and No. DMS-1211713.

[1] P. J. Kedney and F. M. Leslie, Liq. Cryst. **24**, 613 (1998).
[2] A. J. Davidson and N. J. Mottram, Phys. Rev. E **65**, 051710 (2002).
[3] L. J. Cummings, C. Cai, and L. Kondic, J. Eng. Math. **80**, 21 (2013).
[4] L. J. Cummings, C. Cai, and L. Kondic, Phys. Rev. E **88**, 012509 (2013).
[5] G. P. Bryan-Brown, C. V. Brown, J. C. Jones, U. S. Patent No. 6249332 (1995).
[6] E. Willman, F. A. Fernandez, R. James, and S. E. Day, J. Disp. Technol. **4**, 276 (2008).
[7] T. Z. Kosc, Opt. Photonics News **16**, 18 (2005).
[8] V. G. Chigrinov, *Liquid Crystal Devices: Physics and Applications* (Artech House, Boston, 2007).
[9] S. Chandrasekhar, *Liquid Crystals*, 2nd ed. (Cambridge University Press, Cambridge, UK, 1992).
[10] P. G. DeGennes and J. Prost, *The Physics of Liquid Crystals*, 2nd ed., International Series of Monographs on Physics 83 (Oxford University Press, Oxford, UK, 1993).
[11] I. W. Stewart, *The Static and Dynamic Continuum Theory of Liquid Crystals* (Taylor & Francis, London, 2004).
[12] L. M. Blinov, M. Kolovsky, T. Nagata, M. Ozaki, and K. Yoshino, Jpn. J. Appl. Phys. **38**, L1042 (1999).
[13] P. R. M. Murthy, V. A. Raghunathan, and N. V. Madhusudana, Liq. Cryst. **14**, 483 (1993).
[14] A. Rapini and M. Papoular, J. Phys., Colloq. **30**, C4-54 (1969).
[15] C. Cai, Ph.D. thesis, New Jersey Institute of Technology, 2013.
[16] F. M. Leslie, Adv. Liq. Cryst. **4**, 1 (1979).
[17] L. J. Cummings and G. Richardson, Eur. J. Appl. Math. **17**, 435 (2006).
[18] U. Thiele, Eur. Phys. J. Spec. Topics **197**, 213 (2011).